

## **RORyt<sup>+</sup> innate lymphoid cells promote lymph node metastasis of breast cancers.**

Sheeba Irshad<sup>1\*</sup>, Fabian Flores-Borja<sup>1,2\*</sup>, Katherine Lawler<sup>2,3</sup>, James Monypenny<sup>2</sup>, Rachel Evans<sup>2</sup>, Victoria Male<sup>1</sup>, Peter Gordon<sup>1,2</sup>, Anthony Cheung<sup>2</sup>, Patrycja Gazinska<sup>1</sup>, Farzana Noor<sup>1</sup>, Felix Wong<sup>2</sup>, Anita Grigoriadis<sup>1</sup>, Gilbert O Fruhwirth<sup>2, 10</sup>, Paul R Barber<sup>4</sup>, Natalie Woodman<sup>5</sup>, Dominic Patel<sup>11</sup>, Manuel Rodriguez-Justo<sup>11</sup>, Julie Owen<sup>5</sup>, Stewart Martin<sup>6</sup>, Sarah E Pinder<sup>5,7</sup>, Cheryl E. Gillett<sup>5,7</sup>, Simon P Poland<sup>2</sup>, Simon Ameer-Beg<sup>2</sup>, Frank McCaughan<sup>8,9</sup>, Leo M. Carlin<sup>10</sup>, Uzma Hasan<sup>11</sup>, David R Withers<sup>12</sup>, Peter Lane<sup>12</sup>, Borivoj Vojnovic<sup>4</sup>, Sergio A Quezada<sup>13</sup>, Paul Ellis<sup>14</sup>, Andrew Tutt<sup>1, 15</sup> and Tony Ng<sup>1,2,13</sup>.

<sup>1</sup>Breast Cancer Now (BCN) Research Unit, Kings College London (KCL)

<sup>2</sup>Richard Dumbleby, Randall Division & Division of Cancer Studies, KCL

<sup>3</sup> Institute for Mathematical and Molecular Biomedicine, KCL

<sup>4</sup>Gray Institute for Radiation Oncology & Biology, University of Oxford

<sup>5</sup>King's Health Partners Cancer Biobank, KCL

<sup>6</sup>School of Medicine, Division of Cancer and Stem Cells, Department of Clinical Oncology, Nottingham University Hospitals NHS Trust

<sup>7</sup>Research Oncology, Division of Cancer Studies, KCL, 3rd Floor, Bermondsey Wing, Guy's Hospital, London

<sup>8</sup>Department of Asthma, Allergy, and Lung Biology, KCL

<sup>9</sup>Department of Biochemistry, University of Cambridge, Cambridge

<sup>10</sup>Leukocyte Dynamics Group, Beatson Advanced Imaging Resource, CRUK Beatson Institute, Glasgow.

<sup>11</sup>International Center for Infectiology Research, University of Lyon, France

<sup>12</sup>MRC Centre for Immune Regulation, Institute for Biomedical Research, College of Medical and Dental Sciences, University of Birmingham

<sup>13</sup>UCL Cancer Institute, Paul O'Gorman Building, University College London

<sup>14</sup>Department of Medical Oncology, Guy's and St Thomas Foundation Trust, London

<sup>15</sup>ICR, BCN Research Unit, Toby Robins Research Centre, London

Running Title: **ROR $\gamma$ <sup>+</sup> innate lymphoid cells and breast cancer**

Key Words: Innate lymphoid cells, breast cancer, metastasis, LNs, chemokines

\* These authors contributed equally to the manuscript

#Correspondence should be addressed to Professor Tony Ng

Tel: +44(0) 20 7848 8056     e-mail: [tony.ng@kcl.ac.uk](mailto:tony.ng@kcl.ac.uk)

**Conflict of interest statement:** The authors have no conflict of interest to disclose.

Number of Figures: 6

## **Abstract**

Cancer cells tend to metastasize first to tumor-draining lymph nodes (LN), but the mechanisms mediating cancer cell invasion into the lymphatic vasculature remain little understood. Here we show that in the human breast tumor microenvironment (TME) the presence of increased numbers of ROR $\gamma$ <sup>+</sup> group 3 innate lymphoid cells (ILC3) correlates

with an increased likelihood of LN metastasis. In a preclinical mouse model of breast cancer, CCL21-mediated recruitment of ILC3 to tumors stimulated the production of the CXCL13 by TME stromal cells, which in turn promoted ILC3-stromal interactions and production of the cancer cell motile factor RANKL. Depleting ILC3 or neutralizing CCL21, CXCL13 or RANKL was sufficient to decrease LN metastasis. Our findings establish a role for ROR $\gamma$ t+ILC3 in promoting lymphatic metastasis by modulating the local chemokine milieu of cancer cells in the TME.

## **Introduction**

Breast cancer is the most common malignant neoplasm with significant morbidity and mortality. The ability of cancer cells to invade lymphatics stratifies breast cancers into distinct prognostic groups (1). The molecular mechanisms mediating this tumor cell entry remain unclear but studies have established important roles for the lymphoid chemokines CXCL13, CCL19 and CCL21 (2).

An important early step in the construction of lymphoid organs is the recruitment of lymphoid tissue inducer cells (LTis) by CXCL13 and CCL21, which are recognized via the receptors CXCR5 and CCR7, respectively (3-5). LTis are members of the innate lymphoid cells (ILCs) family. Recent moves to propose a uniform nomenclature divide these cells into three groups (6), and LTis represent the prototypic cell type of the “group 3” ROR $\gamma$ t<sup>+</sup> family of ILCs. We will refer to these cells henceforth as ILC3. ILC3 play a major role in lymphoid tissue development both in the embryo (7) and in adult life (8, 9). Within the secondary lymphoid structures, ILC3 produce lymphotoxin (LT) $\alpha_1\beta_2$  which binds LT $\beta$ R on mesenchymal stromal cells (MSC), stimulating the production of CXCL13, CCL19 and CCL21, as well as the tumor necrosis factor (TNF)-family member, RANKL; promoting lymphocyte recruitment and compartmentalization (10).

The presence or role of these cells has not yet been explored in breast cancers. Here we demonstrate that CCL21-dependent recruitment of ILC3s into mammary tumors results in a CXCL13-dependent positive feedback loop between ILC3 and MSCs. Antibody blocking experiments in BALB/c and Rag1<sup>-/-</sup> mice demonstrated that CCL21, CXCL13, ILC3 and RANKL all promote metastasis to the LN. We report the novel identification of RORγt<sup>+</sup>ILC3s within the human TME, their association with more aggressive breast cancer subtypes, and lymphatic metastasis.

## **Methods & Materials**

**Human tissue:** Tissue samples and data from patients were obtained from The King's Health Partners (KHP) Cancer Biobank at Guy's Hospital, London (REC No: 07/40874/131).

**Mice:** Experiments were performed in accordance with the UK Home Office Animals Scientific Procedures Act, 1986 and the UKCCCR guidelines. Tumors were established by injection of 4T1.2 cells into the mammary fat pad of 6–8-week old BALB/c mice (Charles River Laboratories, Wilmington, MA) and Rag1<sup>-/-</sup> mice (BALB/c background, Jackson Laboratories, Bar Harbor, ME). CXCL13 or CCL21 were neutralised by i.v. injection of 0.5ug goat antibodies (R&D Systems, Minneapolis, USA) starting on the first day after tumor establishment and repeated every 3d until the end of the experiment. ILCs were depleted by intraperitoneal injection of 0.25mg anti-CD90.2 (clone 30H12, BioXCell, West Lebanon, USA) starting on d3 after tumor establishment and repeated every 3d until the end of the experiment.

**Gene expression datasets:** The KHP Cancer Biobank of the METABRIC dataset was profiled using the Illumina HT12 platform. Frozen tissue sections were subjected to histopathological review to assess the presence of invasive tumor and only samples with

>70% tumoral DNA were included. Samples were quantile normalised, and a ComBat BeadChip correction applied ( $n=234$ ; 176 ER<sup>+</sup> samples, 58 ER<sup>-</sup> samples). PAM50 subtype was assigned as in (11-13).

***Immunohistochemistry, Immunofluorescence and Image analysis:*** 60 fresh frozen tumor sections were randomly selected from the METABRIC patient cohort for ILC staining as described (14). Confocal tile scan images were obtained using an LSM510 Metamicroscope (Carl Zeiss, UK). Image analysis for ROR $\gamma$ <sup>+</sup>ILC quantification was carried out using MacBiophotonics ImageJ software. Detailed immunohistochemistry protocols are described in Supplementary information.

***Cell Lines and culture conditions:*** The mouse breast cancer cell line 4T1.2 (derived from a mammary carcinoma in a BALB/c mouse) (15) and human bone marrow derived MSC (HS-5) were cultured in DMEM (Invitrogen, Carlsbad, CA) complete media. Extracellular matrix (ECM) invasion assays, based on the Boyden chamber principle, were carried out using 96-well Cell Invasion Assay Kit (ECM555, Chemicon International, CA, USA) as per the manufacturers' instructions. To confirm identity, Short Tandem Repeat (STR) profiling was performed on all cell lines.

***ILC3 cell isolation and flow cytometry:*** For NKp46<sup>-</sup>ILC3 sorting experiments, splenocyte suspensions were prepared from BALB/c mice and cells stained with CD3, CD11c, B220R, CD127, CD90.2 and NKp46 and sorted by using a FACS Aria. The NKp46<sup>-</sup>ILC3 were identified as CD3<sup>-</sup>CD11c<sup>-</sup>B220<sup>-</sup>CD127<sup>+</sup>CD90.2<sup>+</sup>NKp46<sup>-</sup> cells. Purity was confirmed at >90%. To extract intratumoural ILC3, tumors were minced and incubated with collagenase/hyaluronidase at 37°C for 60min; and passed through a filter to form a single cell suspension. Cells were stained as per sorting experiments. Flow cytometry reference beads (PeakFlow blue; Invitrogen) were added to the samples before analysis for quantification of cells in each tumor. The absolute number of cells/mg of tumor was calculated using the

formula: Density of x cells = (number of beads added to each sample multiplied by count of x cells/count of beads)/tumour weight. For multi-photon experiments,  $5\text{--}6 \times 10^4$  sorted NKp46<sup>+</sup> ILC3 were injected (i.v) into tumor-bearing mice on the same day. Immune cell populations from tumors and DLN from mice after treatment with either neutralising anti-CXCL13, anti-CCL21 or IgG control (R&D Systems, Minneapolis, USA) were isolated as described above. Antibodies used are included in Supplementary Table S1.

***Time-lapse microscopy and image analysis:*** Cells were cultured in DMEM complete medium supplemented with 25mM HEPES. For NKp46<sup>+</sup> ILC3-MSc co-culture experiments, MSc were grown in 9.4×10.7 mm ibidi<sup>TM</sup> 8-well-slide chambers. Image acquisition was performed using an Olympus IX71 inverted microscope housed within an environment chamber maintained at 37°C. Sequential phase contrast images were captured every 10-minutes for a total of 10h. NKp46<sup>+</sup> ILC3-MSc clustering was measured as described in Supplementary Information.

***ELISA:*** Tumors were snap frozen and lysed by homogenisation in 100mM Tris pH 7.5, 150mM NaCl, 1mM EGTA, 1mM EDTA, 1% (v/v) Triton-X-100 and 0.5% (w/v) sodium deoxycholate. ELISAs were performed using DuoSet kits (R&D Systems, Minneapolis, USA).

***siRNA knockdown:*** MSc were cultured overnight in 6-well plates to 30% confluency. Cells were transfected with RNAimax in serum free OptiMEM and siRNAs at 20nM. Details of the siRNA used are in Supplementary Table S2.

***Surgical window and Multi-photon Imaging:*** Mammary Imaging Window (MIW) surgery was performed 10d after injection of  $1 \times 10^6$  4T1.2 cells into the mammary fat-pad as described (16). For multi-photon experiments,  $1 \times 10^6$  MSc (control or knock-down) followed 24h later by  $5 \times 10^4$  sorted NKp46<sup>+</sup> ILC3 cells were i.v. injected into mice. 24h later mice were placed in a microscope-attached imaging box kept at 32°C and imaged for a

maximum period of 3h/day for 3 consecutive days. Image processing and image reconstructions were done using MacBiophotonics ImageJ software.

**Statistics:** Permutation tests for small samples with multiple ties were performed using the “coin” package in R-2.13.0 (17). Predictive value of ILC score for high LN burden was determined using Cox’s multivariate proportional hazards model. GraphPad was used for other data analysis. *P* values <0.05 were considered significant.

## Results

### **CCL21-mediated recruitment of NKp46<sup>+</sup>ILC3 to tumors in a mouse model of triple negative breast cancer**

To investigate whether ILC3s are recruited into a TME, we used a mouse model of triple negative breast cancer (TNBC) with 4T1.2 cells in BALB/c mice that develop metastatic disease via lymphatics (Figure 1A) (18). Upon tumor induction, the number of NKp46<sup>+</sup>ILC3 (19) were determined at different times in tumors, draining LN (DLN) and non-draining LN (NDLN) (Figure 1A,B). FACS and immunofluorescence staining for CCR6, ROR $\gamma$ t, and CD4 further confirmed the gated cells to be ILC3 (Supplementary Figure S1). The number of NKp46<sup>+</sup>ILC3 cells in tumors peaked at d14 (d10 vs. d14 *P*=0.0019, unpaired t-test), while the number in DLN peaked later, at d18 (d10 vs. d18, *P*=0.0041 unpaired t-test) (Figure 1B). NKp46<sup>+</sup>ILC3 cell density within the NDLN did not change significantly, acting as an internal control. Confocal imaging of primary tumours and DLNs taken at d14 and d21 respectively, for markers discriminatory for ROR $\gamma$ t<sup>+</sup>ILC3 (defined as ROR $\gamma$ t<sup>+</sup>CD127<sup>+</sup>CD3<sup>-</sup>) as previously published (20) confirmed the presence within our mouse model (Figure 1C and 1D). In contrast to the temporal pattern of NKp46<sup>+</sup>ILC3 infiltration (Figure 1B), absolute numbers of

CD3<sup>+</sup>T cells (Figure 1E) and CD19<sup>+</sup>B cells (Figure 1F) decreased in tumors over time, while the number of T and B cells in the DLN continued to increase until d24.

CXCL13 has an essential role in ILC3 function (5) and lymphoid structures resembling the LN paracortex develop in tumors expressing high levels of CCL21 (21). Therefore, we investigated whether either of these chemokines could play a role in the recruitment of NKp46<sup>+</sup>ILC3 cells to tumors in our model. We confirmed that tumor NKp46<sup>+</sup>ILC3 express both CCR7 and CXCR5, and are thus capable of responding to CCL21 and CXCL13, respectively (Figure 1G). We then analysed the levels of CCL21 and CXCL13 present in primary tumors and serum at various times after tumor establishment. CCL21 levels peaked in both the tumor and serum at d12, before declining rapidly (Figure 1H). CXCL13 in the tumor also peaked early (d10-12), but levels in serum lagged behind, peaking at d14. In contrast to CCL21, CXCL13 oscillated, with tumor CXCL13 beginning to rise again at d20, and serum CXCL13 concentration increasing at d24 (Figure 1I).

To examine the effect of CCL21 or CXCL13 blockade on NKp46<sup>+</sup>ILC3s recruitment to tumors *in vivo*, tumor-bearing mice were treated with control or neutralizing anti-CXCL13 and anti-CCL21 antibodies, starting one day after tumor cell implantation and repeated every 3 days. Tumors were analysed for NKp46<sup>+</sup>ILC3 at d14, a time-point at which maximum number of these cells had previously been shown to be present in the tumors (Figure 1B). When compared with isotype controls, anti-CCL21, but not anti-CXCL13 neutralizing antibodies, significantly reduced NKp46<sup>+</sup>ILC3s recruitment to the primary tumor (Figure 1J).

### **CXCL13 is required for clustering of NKp46<sup>+</sup>ILC3 and MSC**

During embryogenesis clustering of NKp46<sup>+</sup>ILC3s and production of CXCL13 and CCL21 by activated lymphoid tissue organizer cells (LTo, closely linked to stromal cells of mesenchymal origin (22)) are responsible for initiating a feedback loop with further NKp46<sup>+</sup>



ILC3 recruitment and subsequent amplification of LT-receptor signaling (23). Given the lineage relationship between MSCs, which exhibit a marked tropism for tumors (24), and LTo cells that are known to interact with ILC3s, we hypothesized that ILC3 interaction with CXCL13-producing stromal cells may modulate the chemokine profile of the TME. Within our *in-vitro* model, MSCs secrete high concentrations of CCL21 and CXCL13 chemokines (Supplementary Figure S2).

Time-lapse microscopy demonstrated NKp46<sup>+</sup>ILC3-MSC clustering (Figure 2A, upper panel and Video S1), with cells remaining closely associated for as long as 7h (Figure 2A, red arrow in lower panel and Video S2). There was no effect on proliferation of ILC3 on contact or co-culture with MSCs (Supplementary Figure S3A). We quantified cell clustering of NKp46<sup>+</sup>ILC3-MSC (Figure 2B) and investigated how knockdown of CXCL13 and CCL21 in MSC (Supplementary Figure S3B and C) affected this clustering rate. Transient siRNA-knockdown of CXCL13, but not of CCL21, resulted in a decrease of NKp46<sup>+</sup>ILC3-MSC clustering around ( $P<0.0001$ , unpaired t-test) (Figure 2C). CXCL13-mediated clustering may be synergistic with the initial CCL21-mediated recruitment of NKp46<sup>+</sup>ILC3 into the primary tumor, since the CCL21-recruited NKp46<sup>+</sup>ILC3 are required to promote significant CXCL13 production by interaction with MSC.

Next, we used an intravital mammary window (MIW) with multi-photon imaging to assess NKp46<sup>+</sup>ILC3-MSC interaction *in vivo* (16). These visualisation experiments were conducted to demonstrate how the fluorescent MSC (which are allogenic and therefore could have a finite half-life once injected *in vivo*) may interact with ILC in the relatively short term and whether this interaction is CXCL13 dependent. 4T1.2 cells were injected into the mammary fat pad and a MIW placed over the tumor 10d after inoculation (Figure 2Di). Tumor-bearing mice were treated with either neutralizing anti-CXCL13 or isotype antibody (as described for Figure 1H). Fluorescently-labeled MSCs and NKp46<sup>+</sup>ILC3 were i.v. injected 48 or 24h prior

to imaging, respectively (Figure 2Dii). In control antibody-treated mice, NKp46<sup>+</sup>ILC3 were clustered and in close proximity to MSC. However, in mice injected with neutralizing anti-CXCL13 antibody, NKp46<sup>+</sup>ILC3 and MSC were not close with each other ( $P<0.0001$ , unpaired t-test, Figure 2E, F). These *in vivo* imaging results support the *in vitro* observation that NKp46<sup>+</sup>ILC3-MSK clustering is CXCL13-dependent.

### **CCL21, CXCL13 and NKp46<sup>+</sup>ILC3 cells promote metastasis of tumor cells to DLN**

To test the hypothesis that CCL21 and CXCL13 might play a role in promoting metastasis of tumor cells to LN, we treated 4T1.2 tumor-bearing mice with neutralising antibodies against CCL21 or CXCL13, or with an antibody to deplete NKp46<sup>+</sup>ILC3 and examined the DLN for evidence of metastasis.

*In vivo*, neither anti-CXCL13 nor anti-CCL21 treatments affected tumour growth (Figure 3A). The weight of the DLNs were significantly reduced in both cohorts (anti-CXCL13  $P=0.0156$ ; and anti-CCL21  $P=0.0017$  one-way ANOVA) compared to the control cohort (Figure 3B). Immunohistochemical analysis of DLN for tumor load with anti-pancytokeratin revealed fewer tumor foci within the DLN of mice treated with anti-CXCL13 or anti-CCL21 compared with control antibody-treated mice (Figure 3C). Measurements of the total surface area of tumor foci ( $\mu\text{m}^2$ ) demonstrated a significant decrease in the tumor load in the DLN of mice treated with anti-CXCL13 or anti-CCL21 ( $P<0.05$  one-way ANOVA; Figure 3C and 3D).

Given the involvement of CXCL13 and CCL21 in B- and T-cell homeostasis (2), we assessed the effect of anti-CXCL13 and anti-CCL21 blockade on LN metastasis in Rag1<sup>-/-</sup> mice which lack B and T cells. Rag1<sup>-/-</sup> mice have much smaller lymph nodes, these lymph nodes samples were therefore formalin fixed to help preserve the morphology better. We report a decrease

in the number of pan-cytokeratin positive tumour cells in DLN of tumor-bearing Rag1<sup>-/-</sup> mice treated with blocking anti-CCL21 or anti-CXCL13 (anti-CXCL13  $P=0.004$ ; anti-CCL21  $P=0.005$ ) (Figure 3E & 3F). These results suggest that T and B cells are not involved in the CXCL13 and CCL21 dependent tumor cell migration into LNs.

To strengthen the link between ILC and chemokines in LN metastasis we depleted ILCs with anti-CD90.2, as previously described (25) (Figure 3G). It is noteworthy that anti-CD90.2 does not specifically deplete ILC3 and is also able to deplete T cells. Therefore these experiments were also carried out in Rag1<sup>-/-</sup> mice. We found a significant decrease in the tumor burden in the DLN of mice treated with anti-CD90.2 ( $P=0.04$  Mann Whitney test Figure 3H). Therefore, CCL21, CXCL13 and ILCs themselves, and not B or T cells, all promote metastasis of breast cancer cells to the DLN.

### **CXCL13 induces RANK/RANKL signalling to promote tumour cell invasion**

As our *in vivo* results suggested an inhibitory effect of CXCL13 or CCL21 blockade on 4T1.2 cell invasion into the DLN, we used extracellular matrix (ECM) invasion assay, to directly investigate the effects of increasing concentrations of CXCL13 and CCL21 on tumour cell invasion. EGF stimulation of 4T1.2 and NIH3T3 served as positive and negative controls respectively. Recombinant CXCL13 or CCL21 did not significantly increase the invasion of 4T1.2 cells at concentrations between 10-100ng/ml (Figure 4A).

During LN development, the interaction of NKp46<sup>+</sup>ILC3-MSc stimulates RANKL production by MSc, and RANKL signals back to the NKp46<sup>+</sup>ILC3 establishing a positive feedback (26). CXCL13 has recently been shown to promote RANKL expression in stromal cells in oral squamous cell carcinoma (27); and RANK signaling in several breast cancer cell lines induces epithelial-mesenchymal transition, promoting cell migration and invasion (28).

To test the relationship between CXCL13 and RANK signaling *in vitro*; we first confirmed, as shown previously (27), that whilst 4T1.2 cells expressed RANK receptor *in vitro* (Figure 4B), but were not themselves the source of RANKL (Figure 4C). Levels of over 200pg/ml of RANKL were observed in MSC conditioned media, supporting the hypothesis that the source of RANKL within the tumour is likely to be stromal (Figure 4C). Stimulation with CXCL13, but not CCL21, increased the expression of RANKL in MSC (paired t-test 50ng/ml vs control:  $P<0.01$ ; Figure 4D & 4E). We also confirmed that MSCs expressed CXCR5 as suggested by the above experiment (Supplementary Figure S4). We next investigated if increasing concentrations of RANKL would increase 4T1.2 cells invasion. Addition of RANKL to 4T1.2 (between 10-100ng/ml) was observed to significantly increase the ability of the tumour cells to invade through the matrix (Figure 4F).

To investigate the relationship between CXCL13 and RANKL expression *in vivo*, we analysed the changes in the levels of RANKL in the sera of 4T1.2 tumor-bearing mice at a number of timepoints after tumor establishment. RANKL levels peaked at d18 ( $P<0.0001$ , unpaired t-test; Figure 4G), approximately 4d after the first serum peak in CXCL13 (Figure 1H). In mice treated with anti-CXCL13, levels of RANKL at d14 were significantly reduced ( $P<0.001$  unpaired t-test; Figure 4H), in support of the idea that CXCL13 drives RANKL production *in vivo*. A significant reduction in RANKL was also observed in anti-CCL21 treated mice ( $P<0.001$  unpaired t-test; Figure 4H).

These findings led us to hypothesise that RANKL, like CCL21 and CXCL13, might promote metastasis of tumor cells to DLN. Treatment with anti-RANKL neutralizing antibody did not affect the growth of the primary tumor (Figure 4I). Immunohistochemical analysis of DLN for tumor load revealed no metastasis in majority of antibody-treated mice ( $n = 5/7$ ) and the mean area of tumor metastasis was lower in the antibody-treated mice than the controls ( $P<0.01$ , unpaired t-test; Figure 4J). RANKL blockade using a neutralising antibody did not

significantly affect the recruitment of NKp46<sup>+</sup>ILC3 into the primary tumors but the numbers in DLN were significantly lower, compared to the controls ( $P<0.05$ , one-way ANOVA; Figure 4K).

### **ROR $\gamma$ t<sup>+</sup>ILC and their associated chemokines are present in the human breast cancer TME**

We further analysed the gene expression of ROR $\gamma$ t<sup>+</sup>ILC3-associated/lymphoid chemokines CXCL13, CCL19, and CCL21 and their receptors, CXCR5 and CCR7, in a subset of 234 samples of breast cancer from the Molecular Taxonomy of Breast Cancer International Consortium (METABRIC) (29) (see Supplementary Table S3 for patient characteristics). Unsupervised hierarchical cluster analysis of the transcriptional profile in these samples revealed that this cohort could be categorized based on their expression of ROR $\gamma$ t<sup>+</sup>ILC3-associated/lymphoid chemokines and their receptors (Figure 5A). “Basal-like” breast cancers (PAM50 intrinsic subtype assignments (30)) presented high expression of these genes (31/53 basal-like tumors lie in the top-branch cluster,  $n=89$ ;  $P=0.0007$ , two-tailed Fisher's exact test) (Figure 5A). Further cross validation of these results was seen in 4-independent breast cancer datasets (Supplementary Figure S5). ROR $\gamma$ t<sup>+</sup>ILC3-associated/lymphoid chemokine and their receptor genes were highly specific (no association with other lymphoid chemokine genes, such as the ligand-receptor pair CCL20-CCR6, which attract immature DC, effector/memory T-cells and B-cells) and showed significant internal pair-wise correlation ( $P<10^{-4}$ , Figure 5B).

We next stained frozen primary tumor sections for markers for ROR $\gamma$ t<sup>+</sup>ILC3 (defined as ROR $\gamma$ t<sup>+</sup>CD127<sup>+</sup>CD3<sup>-</sup>), as we previously published (20). ROR $\gamma$ t<sup>+</sup>ILC3 were present in approximately half of the sections examined (Figure 5C, 5D). These cells were in proximity

to CD3<sup>+</sup>T cells (Figure 5C) and found within TLS, as previously defined (31) (Supplementary Figure S6). We hypothesized that tumors with higher levels of RORγt<sup>+</sup>ILC3-associated chemokines would have a higher number of RORγt<sup>+</sup>ILC3. To test this, we performed a blinded study in primary breast cancer sections (total patients *n*=59). The number of RORγt<sup>+</sup>CD127<sup>+</sup>CD3<sup>-</sup> cells/mm<sup>2</sup> (of total area/section) varied considerably from case to case (range 0–56/mm<sup>2</sup>) (Figure 5D) but patients with high tumor ILC3 counts were also likely to have a high gene expression score for the ILC3-associated chemokines (Figure 5D; *P*<0.001, Spearman correlation permutation test).

We next assessed the correlation of CXCL13 and CCL21 protein and gene expression levels with ILC3 scores. Fifty-nine cases with known ILC3 scores were stained for CXCL13 or CCL21 expression. For CXCL13 only stromal cells stained for this chemokine (Figure 5Ei). In contrast, CCL21 staining was positive for both tumoral and stromal cells. We quantified the relationship between ILC3 and stromal CXCL13/CCL21 staining. ILC3 presence correlated positively with CXCL13 staining but not with stromal CCL21 (Figure 5Eii). These additional data strengthen our pre-clinical data (Figure 2), with CXCL13 up-regulation in stromal cells as a secondary event to the recruitment of ILC3 to the primary tumour.

### **Tumoral RORγt<sup>+</sup>ILC3 cell density correlates with lymphatic tumor cell invasion and DLN metastasis within basal-like and HER2-enriched breast cancer**

We next stained tumor sections for the lymphatic endothelial cell marker, podoplanin, and evaluated sections for evidence of tumor cell invasion into lymphatics (Figure 6Ai). We considered lymphatic invasion to have occurred if at least one tumor cell cluster was clearly visible in the lymphatic vascular space (red arrow in Figure 6Ai). RORγt<sup>+</sup>ILC3 were present in 82% (14/17) of tumor samples with lymphatic tumor cell invasion but only in 27% (8/30)

of samples without lymphatic tumor cell invasion. Similarly, 73% (22/30) of samples without lymphatic tumor cell invasion had no ROR $\gamma$ <sup>+</sup>ILC3 present in the tumor, whereas only 17% (3/17) of samples without ROR $\gamma$ <sup>+</sup>ILC3 cells displayed lymphatic invasion (Figure 6ii;  $P<0.003$ , Fisher's exact test). We did not find an association between lymphatic invasion and CD3<sup>+</sup>T cells or with CD3<sup>+</sup>CD127<sup>+</sup>ROR $\gamma$ <sup>+</sup> (most likely representing TH17 cells), strengthening the specificity of the correlation between ROR $\gamma$ <sup>+</sup>ILC3 cells and lymphatic invasion (Table 2). We next investigated if the association between ROR $\gamma$ <sup>+</sup>ILC3 counts and lymphatic invasion translated into a high LN tumour burden (i.e. four or more metastatic LNs at surgical resection) within our dataset. In basal-like breast cancer raised ROR $\gamma$ <sup>+</sup>ILC3 counts were found to also correlate with a higher burden of LN metastases ( $P=0.02$ , permutation-based Mann–Whitney; Figure 6B). Given our *in vitro* and *in vivo* findings, we investigated whether LN burden was related to gene expression of CCL21 and CXCL13 in the primary tumor. We found that in basal-like breast cancers a high LN tumor burden was associated with significantly increased levels of CCL21 ( $P=0.0043$ ; LN positive, 4+ vs. 0; two-tailed Mann–Whitney; Figure 6C). Although CXCL13 levels were also increased in patients suffering from a high LN burden, this association was not significant ( $P=0.15$ ; Figure 6D). These correlations were not statistically significant in other breast cancer subtypes (HER2+ve or Luminal A/B), suggesting that the proposed mechanisms may only operate in specific breast cancer subtypes. In a multivariate (Cox's) proportional hazards model and taking basal-like and HER2-enriched tumors together, the ROR $\gamma$ <sup>+</sup>ILC3 score achieved 84% prediction accuracy for high LN burden: higher than traditional clinicopathological parameters (e.g. grade, tumor size, receptor status; Figure 6E).

## Discussion

Recent years have seen a growing appreciation of the pleiotropic nature of the TME (32). The importance of ILC3s in normal lymphoid organogenesis has been accepted for long time but their role in the TME has only recently begun to be investigated. Work by Shields *et al* described, in a murine model of melanoma, a mechanism by which CCL21-expressing tumors recruit ILC3 cells, which transform the TME contributing to a tolerant milieu that promotes immune evasion (21). Study by Eisenring *et al* showed that ROR $\gamma$ <sup>+</sup>ILCs, are required for IL-12 to exert its anti-tumor activity (33). Similarly, a protective function of NKp46<sup>+</sup>ILC3 (distinct from the NKp46<sup>-</sup>ILC3) has been reported in lung cancers (34). These findings are not necessarily at odds, since whether ILC3s promote or prevent cancer progression is likely to depend on the type of cancer and whether they recruit immune cells into a tolerogenic (21) or inflammatory (33) microenvironment. We report the presence of ROR $\gamma$ <sup>+</sup>ILC3 in human breast cancers and that they have a previously unrecognized function in facilitating tumor invasion into the lymphatic system through modulation of the local lymphoid chemokine milieu. We show that ILC3 recruitment into a TNBC tumor model is CCL21-dependent, whilst CXCL13 regulates their clustering with stromal cells (see Figure 7).

The CCL21/CCR7 axis plays a role in the progression of different malignancies (35, 36). These studies focus on the direct effects of CCL21 on CCR7-expressing tumor cells, rather than on how CCL21 may modify the TME. We show that CCL21 is expressed both in primary human breast cancers and in a mouse model of TNBC. In the mouse model, the peak of CCL21 expression in tumors was closely followed by ILC3 recruitment, an association we show to be causal through its prevention by CCL21 blockade, consistent with the melanoma xenograft study correlating tumor expression of CCL21 and ILC3 cells recruitment (21).



CXCL13 was not required for ILC3 recruitment to tumors but was important for the induction of ILC3-MSK clustering and RANKL upregulation by MSC. MSC are recruited to tumors early in development via mechanisms reminiscent of those that operate in chronic wound healing (37, 38). Once activated, they secrete CXCL13, CCL21 and CCL19 and secrete lymphangiogenic factors such as VEGF-C (39). This interaction, in the TME, may promote neo-lymphangiogenesis, increasing the number of lymphatic vessels into which tumor cells are able to migrate and thus increasing opportunities for lymphatic metastases.

In addition to its role in promoting clustering, CXCL13 stimulates increased RANKL production by MSC. This is likely to facilitate DLN metastasis by promoting epithelial-mesenchymal transition in breast cancer cells, enhancing their ability to migrate and metastasize (28, 40). This explains the reduction in serum levels of RANKL observed in anti-CXCL13 treated mice. ILC3 interaction with CXCL13-producing stromal cells may constitute a positive feedback, with CXCL13 reinforcing the ILC3-MSK interaction as shown *in vitro* and by intravital imaging. These are likely to explain our observations that patients with tumor cell invasion into the lymphatics were more likely to have a higher ROR $\gamma$ <sup>+</sup>ILC3 score compared to patients without lymphatic vessel invasion, as well as the significant association between ROR $\gamma$ <sup>+</sup>ILC3 counts and greater risk of an increased number of LN metastasis in basal-like breast cancer patients.

CXCL13 is highly expressed in clinical samples from some breast cancer patients (41) but there is conflicting evidence on how it affects disease progression. While high CXCL13-CXCR5 expression positively correlate with classical determinants of poor prognosis (41, 42), it serves as a good prognostic marker within this high-risk subgroup of breast cancer patients (42-44). Within the TME, the role of immune cells and/or chemokines is particularly complex (45, 46). Here, we report that, downstream of CCL21-mediated recruitment of

intra-tumoral ILC3, CXCL13 promotes lymphatic invasion of tumor cells via the RANK-RANKL signalling pathway. However, CXCL13 is also a powerful chemoattractant for lymphocytes (47). This is in line with our finding that basal-like breast cancers, which frequently bear a prominent lymphocytic infiltrate, presented a high score for the lymphoid chemokine/chemokine receptor gene signature, and our data demonstrating a decreased number of tumor-infiltrating lymphocytes (TILs) in anti-CCL21 or anti-CXCL13-treated mice. Additionally, the presence of TILs and TLS are described as key prognostic and predictive markers for specific breast cancer subtypes (47-50). Therefore, the well-established role of CXCL13 as a chemoattractant could explain why, in a subset of cases, it seems to play a protective role. In our cohort of patients, CCL21 expression and ROR $\gamma$ <sup>+</sup>ILC3 presence in the primary tumor were associated with increased DLN metastasis in basal-like breast cancer, but not in HER2+ve or luminalA/B subtypes. It is noteworthy that these data may not translate into worse prognosis for patients and additional studies are required to fully understand the clinical significance of these findings.

One important consideration for any future development of chemokine-based therapeutic interventions is the interplay between the CCL19-CCL21/CCR7 and CXCL13/CXCR5 axes within tumors. Both have been implicated as important drivers of leukocyte trafficking and lymphoid organogenesis in physiological situations (51). However, it is important to make a distinction between the two chemokines in the pathological context of the TME since CXCL13, but not CCL21, is required for ILC3-MSCs clustering, which we proposed here to be an important regulatory mechanism in tumor cell migration through RANKL production by MSC.

In summary, we propose that, in our tumor model, ILC3 are recruited to the tumor by CCL21, have a pivotal role in facilitating lymphatic vessel invasion by tumor cells and they do this

via two CXCL13-mediated positive feedback loops. Further investigation into how ILC3, MSC, CCL21, CXCL13 and RANKL are co-ordinated to establish a network of interactions between the tumor cells and their microenvironment is required.

## References

1. Mohammed RA, Ellis IO, Mahmmud AM, Hawkes EC, Green AR, Rakha EA, et al. Lymphatic and blood vessels in basal and triple-negative breast cancers: characteristics and prognostic significance. *Mod Pathol*. 2011 Jun;24(6):774-85. PubMed PMID: 21378756. Epub 2011/03/08. eng.
2. Stein JV, Nombela-Arrieta C. Chemokine control of lymphocyte trafficking: a general overview. *Immunology*. 2005 Sep;116(1):1-12. PubMed PMID: 16108812. Pubmed Central PMCID: 1802414. Epub 2005/08/20. eng.
3. Ansel KM, Ngo VN, Hyman PL, Luther SA, Forster R, Sedgwick JD, et al. A chemokine-driven positive feedback loop organizes lymphoid follicles. *Nature*. 2000 Jul 20;406(6793):309-14. PubMed PMID: 10917533. Epub 2000/08/05. eng.
4. Ohl L, Henning G, Krautwald S, Lipp M, Hardtke S, Bernhardt G, et al. Cooperating mechanisms of CXCR5 and CCR7 in development and organization of secondary lymphoid organs. *The Journal of experimental medicine*. 2003 May 5;197(9):1199-204. PubMed PMID: 12732661. Pubmed Central PMCID: Pmc2193963. Epub 2003/05/07. eng.
5. van de Pavert SA, Olivier BJ, Goverse G, Vondenhoff MF, Greuter M, Beke P, et al. Chemokine CXCL13 is essential for lymph node initiation and is induced by retinoic acid and neuronal stimulation. *Nat Immunol*. 2009 Nov;10(11):1193-9. PubMed PMID: 19783990. Pubmed Central PMCID: 2771164.
6. Spits H, Artis D, Colonna M, Diefenbach A, Di Santo JP, Eberl G, et al. Innate lymphoid cells--a proposal for uniform nomenclature. *Nature reviews Immunology*. 2013 Feb;13(2):145-9. PubMed PMID: 23348417.
7. Sun Z, Unutmaz D, Zou YR, Sunshine MJ, Pierani A, Brenner-Morton S, et al. Requirement for RORgamma in thymocyte survival and lymphoid organ development. *Science (New York, NY)*. 2000 Jun 30;288(5475):2369-73. PubMed PMID: 10875923. Epub 2000/07/06. eng.
8. Tsuji M, Suzuki K, Kitamura H, Maruya M, Kinoshita K, Ivanov, II, et al. Requirement for lymphoid tissue-inducer cells in isolated follicle formation and T cell-independent immunoglobulin A generation in the gut. *Immunity*. 2008 Aug 15;29(2):261-71. PubMed PMID: 18656387. Epub 2008/07/29. eng.
9. Scandella E, Bolinger B, Lattmann E, Miller S, Favre S, Littman DR, et al. Restoration of lymphoid organ integrity through the interaction of lymphoid tissue-inducer cells with stroma of the T cell zone. *Nat Immunol*. 2008 Jun;9(6):667-75. PubMed PMID: 18425132. Epub 2008/04/22. eng.
10. Honda K, Nakano H, Yoshida H, Nishikawa S, Rennert P, Ikuta K, et al. Molecular basis for hematopoietic/mesenchymal interaction during initiation of Peyer's patch organogenesis. *The Journal of experimental medicine*. 2001 Mar 5;193(5):621-30. PubMed PMID: 11238592. Pubmed Central PMCID: Pmc2193398. Epub 2001/03/10. eng.
11. Weigelt B, Mackay A, A'Hern R, Natrajan R, Tan DS, Dowsett M, et al. Breast cancer molecular profiling with single sample predictors: a retrospective analysis. *The lancet oncology*. 2010 Apr;11(4):339-49. PubMed PMID: 20181526.
12. Parker JS, Mullins M, Cheang MC, Leung S, Voduc D, Vickery T, et al. Supervised risk predictor of breast cancer based on intrinsic subtypes. *Journal of clinical oncology : official journal of the American Society of Clinical Oncology*. 2009 Mar 10;27(8):1160-7. PubMed PMID: 19204204. Pubmed Central PMCID: 2667820.

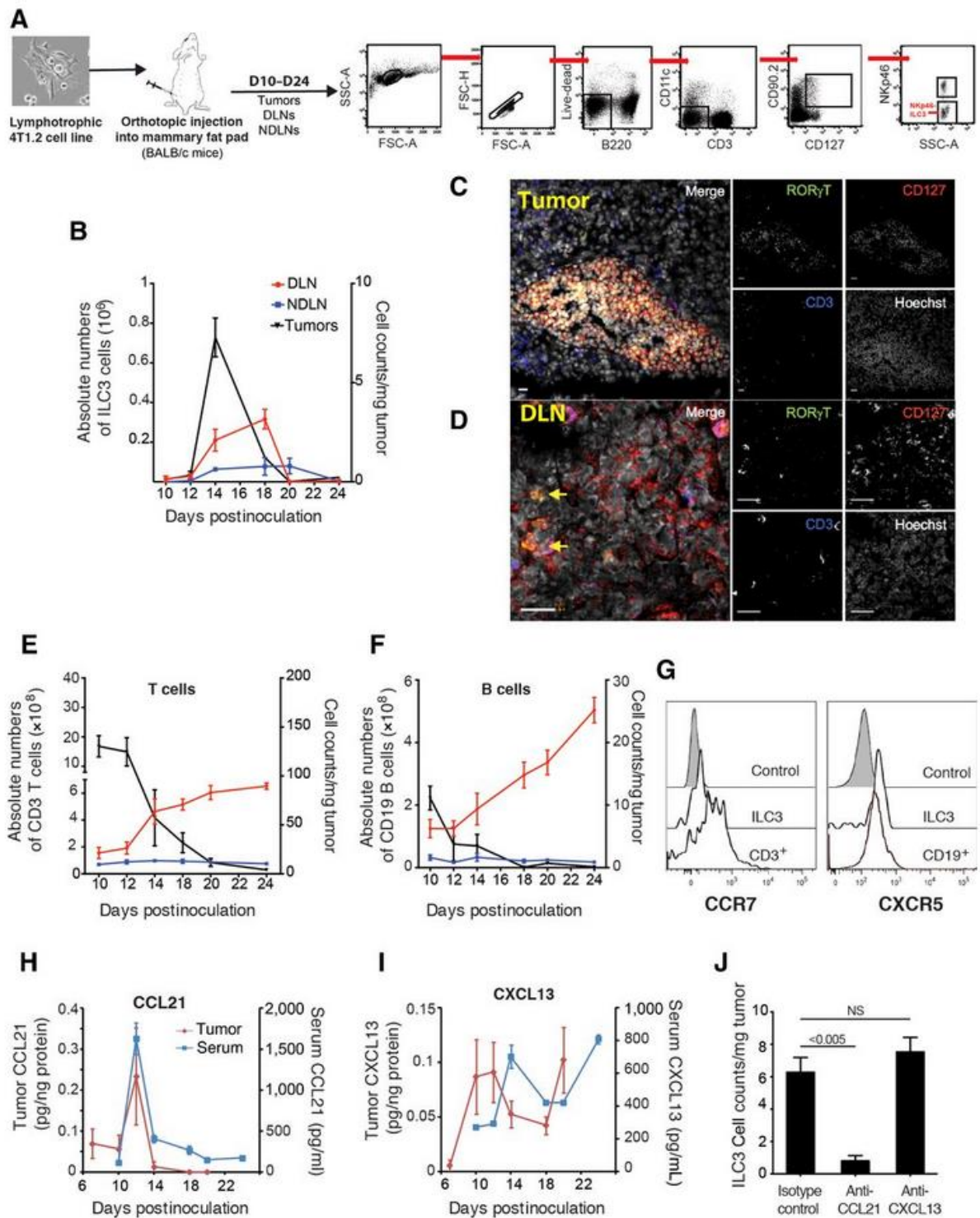
13. Gazinska P, Grigoriadis A, Brown JP, Millis RR, Mera A, Gillett CE, et al. Comparison of basal-like triple-negative breast cancer defined by morphology, immunohistochemistry and transcriptional profiles. *Modern pathology : an official journal of the United States and Canadian Academy of Pathology, Inc.* 2013 Jul;26(7):955-66. PubMed PMID: 23392436.
14. Withers DR, Gaspal FM, Mackley EC, Marriott CL, Ross EA, Desanti GE, et al. Cutting edge: lymphoid tissue inducer cells maintain memory CD4 T cells within secondary lymphoid tissue. *Journal of immunology (Baltimore, Md : 1950).* 2012 Sep 1;189(5):2094-8. PubMed PMID: 22855716. Pubmed Central PMCID: 3442242.
15. Lelekakis M, Moseley JM, Martin TJ, Hards D, Williams E, Ho P, et al. A novel orthotopic model of breast cancer metastasis to bone. *Clinical & experimental metastasis.* 1999 Mar;17(2):163-70. PubMed PMID: 10411109.
16. Kedrin D, Gligorijevic B, Wyckoff J, Verkhusha VV, Condeelis J, Segall JE, et al. Intravital imaging of metastatic behavior through a mammary imaging window. *Nat Methods.* 2008 Dec;5(12):1019-21. PubMed PMID: 18997781. Pubmed Central PMCID: 2820719.
17. Hothorn T HK, van de Wiel MA, Zeileis A A Lego System for Conditional Inference. *The American Statistician.* 2006;60(3):257-63.
18. Kaur P, Nagaraja GM, Zheng H, Gizachew D, Galukande M, Krishnan S, et al. A mouse model for triple-negative breast cancer tumor-initiating cells (TNBC-TICs) exhibits similar aggressive phenotype to the human disease. *BMC cancer.* 2012;12:120. PubMed PMID: 22452810. Pubmed Central PMCID: Pmc3340297. Epub 2012/03/29. eng.
19. Walker JA, Barlow JL, McKenzie AN. Innate lymphoid cells--how did we miss them? *Nature reviews Immunology.* 2013 Feb;13(2):75-87. PubMed PMID: 23292121.
20. Kim S, Han S, Withers DR, Gaspal F, Bae J, Baik S, et al. CD117(+) CD3(-) CD56(-) OX40Lhigh cells express IL-22 and display an LT $\alpha$ i phenotype in human secondary lymphoid tissues. *Eur J Immunol.* 2011 Jun;41(6):1563-72. PubMed PMID: 21469096.
21. Shields JD, Kourtis IC, Tomei AA, Roberts JM, Swartz MA. Induction of lymphoidlike stroma and immune escape by tumors that express the chemokine CCL21. *Science (New York, NY).* 2010 May 7;328(5979):749-52. PubMed PMID: 20339029. Epub 2010/03/27. eng.
22. Brendolan A, Caamano JH. Mesenchymal cell differentiation during lymph node organogenesis. *Frontiers in immunology.* 2012;3:381. PubMed PMID: 23248630. Pubmed Central PMCID: 3522075.
23. Evans I, Kim MY. Involvement of lymphoid inducer cells in the development of secondary and tertiary lymphoid structure. *BMB Rep.* 2009 Apr 30;42(4):189-93. PubMed PMID: 19403040.
24. Bernardo ME, Locatelli F, Fibbe WE. Mesenchymal Stromal Cells. *Annals of the New York Academy of Sciences.* 2009;1176(1):101-17.
25. Monticelli LA, Sonnenberg GF, Abt MC, Alenghat T, Ziegler CG, Doering TA, et al. Innate lymphoid cells promote lung-tissue homeostasis after infection with influenza virus. *Nature immunology.* 2011 Nov;12(11):1045-54. PubMed PMID: 21946417. Pubmed Central PMCID: 3320042.
26. Mueller CG, Hess E. Emerging Functions of RANKL in Lymphoid Tissues. *Frontiers in immunology.* 2012;3:261. PubMed PMID: 22969763. Pubmed Central PMCID: Pmc3432452. Epub 2012/09/13. eng.

27. Sambandam Y, Sundaram K, Liu A, Kirkwood KL, Ries WL, Reddy SV. CXCL13 activation of c-Myc induces RANK ligand expression in stromal/preosteoblast cells in the oral squamous cell carcinoma tumor-bone microenvironment. *Oncogene*. 2013 Jan 3;32(1):97-105. PubMed PMID: 22330139. Pubmed Central PMCID: Pmc3355224. Epub 2012/02/15. eng.
28. Palafox M, Ferrer I, Pellegrini P, Vila S, Hernandez-Ortega S, Urruticoechea A, et al. RANK induces epithelial-mesenchymal transition and stemness in human mammary epithelial cells and promotes tumorigenesis and metastasis. *Cancer Res*. 2012 Jun 1;72(11):2879-88. PubMed PMID: 22496457.
29. Curtis C, Shah SP, Chin SF, Turashvili G, Rueda OM, Dunning MJ, et al. The genomic and transcriptomic architecture of 2,000 breast tumours reveals novel subgroups. *Nature*. 2012 Jun 21;486(7403):346-52. PubMed PMID: 22522925. Pubmed Central PMCID: 3440846.
30. Perou CM, Sorlie T, Eisen MB, van de Rijn M, Jeffrey SS, Rees CA, et al. Molecular portraits of human breast tumours. *Nature*. 2000 Aug 17;406(6797):747-52. PubMed PMID: 10963602.
31. Pages F, Galon J, Dieu-Nosjean MC, Tartour E, Sautes-Fridman C, Fridman WH. Immune infiltration in human tumors: a prognostic factor that should not be ignored. *Oncogene*. 2010 Feb 25;29(8):1093-102. PubMed PMID: 19946335. Epub 2009/12/01. eng.
32. Quail DF, Joyce JA. Microenvironmental regulation of tumor progression and metastasis. *Nat Med*. 2013 Nov;19(11):1423-37. PubMed PMID: 24202395.
33. Eisenring M, vom Berg J, Kristiansen G, Saller E, Becher B. IL-12 initiates tumor rejection via lymphoid tissue-inducer cells bearing the natural cytotoxicity receptor NKp46. *Nature immunology*. 2010 Nov;11(11):1030-8. PubMed PMID: 20935648. Epub 2010/10/12. eng.
34. Carrega P, Loiacono F, Di Carlo E, Scaramuccia A, Mora M, Conte R, et al. NCR(+)ILC3 concentrate in human lung cancer and associate with intratumoral lymphoid structures. *Nature communications*. 2015;6:8280. PubMed PMID: 26395069.
35. Mashino K, Sadanaga N, Yamaguchi H, Tanaka F, Ohta M, Shibuta K, et al. Expression of chemokine receptor CCR7 is associated with lymph node metastasis of gastric carcinoma. *Cancer research*. 2002 May 15;62(10):2937-41. PubMed PMID: 12019175. Epub 2002/05/23. eng.
36. Muller A, Homey B, Soto H, Ge N, Catron D, Buchanan ME, et al. Involvement of chemokine receptors in breast cancer metastasis. *Nature*. 2001 Mar 1;410(6824):50-6. PubMed PMID: 11242036. Epub 2001/03/10. eng.
37. Spaeth E, Klopp A, Dembinski J, Andreeff M, Marini F. Inflammation and tumor microenvironments: defining the migratory itinerary of mesenchymal stem cells. *Gene Ther*. 2008 May;15(10):730-8. PubMed PMID: 18401438.
38. Dvorak HF. Tumors: wounds that do not heal. Similarities between tumor stroma generation and wound healing. *N Engl J Med*. 1986 Dec 25;315(26):1650-9. PubMed PMID: 3537791.
39. Benezech C, White A, Mader E, Serre K, Parnell S, Pfeffer K, et al. Ontogeny of stromal organizer cells during lymph node development. *Journal of immunology (Baltimore, Md : 1950)*. 2010 Apr 15;184(8):4521-30. PubMed PMID: 20237296. Pubmed Central PMCID: Pmc2862734. Epub 2010/03/20. eng.
40. Biswas S, Sengupta S, Roy Chowdhury S, Jana S, Mandal G, Mandal PK, et al. CXCL13-CXCR5 co-expression regulates epithelial to mesenchymal transition of breast cancer cells during lymph node metastasis. *Breast cancer research and*

- treatment. 2014 Jan;143(2):265-76. PubMed PMID: 24337540. Epub 2013/12/18. eng.
41. Panse J, Friedrichs K, Marx A, Hildebrandt Y, Luetkens T, Barrels K, et al. Chemokine CXCL13 is overexpressed in the tumour tissue and in the peripheral blood of breast cancer patients. *Br J Cancer*. 2008 Sep 16;99(6):930-8. PubMed PMID: 18781150. Pubmed Central PMCID: 2538749.
  42. Razis E, Kalogeras KT, Kotoula V, Eleftheraki AG, Nikitas N, Kronenwett R, et al. Improved outcome of high-risk early HER2 positive breast cancer with high CXCL13-CXCR5 messenger RNA expression. *Clin Breast Cancer*. 2012 Jun;12(3):183-93. PubMed PMID: 22607768.
  43. Yau C, Esserman L, Moore DH, Waldman F, Sninsky J, Benz CC. A multigene predictor of metastatic outcome in early stage hormone receptor-negative and triple-negative breast cancer. *Breast Cancer Res*. 2010;12(5):R85. PubMed PMID: 20946665. Pubmed Central PMCID: 3096978.
  44. Sabatier R, Finetti P, Mamessier E, Raynaud S, Cervera N, Lambaudie E, et al. Kinome expression profiling and prognosis of basal breast cancers. *Mol Cancer*. 2011;10:86. PubMed PMID: 21777462. Pubmed Central PMCID: 3156788.
  45. DeNardo DG, Andreu P, Coussens LM. Interactions between lymphocytes and myeloid cells regulate pro- versus anti-tumor immunity. *Cancer metastasis reviews*. 2010 Jun;29(2):309-16. PubMed PMID: 20405169. Pubmed Central PMCID: Pmc2865635. Epub 2010/04/21. eng.
  46. Viola A, Sarukhan A, Bronte V, Molon B. The pros and cons of chemokines in tumor immunology. *Trends in immunology*. 2012 Oct;33(10):496-504. PubMed PMID: 22726608. Epub 2012/06/26. eng.
  47. Gu-Trantien C, Loi S, Garaud S, Equeter C, Libin M, de Wind A, et al. CD4+ follicular helper T cell infiltration predicts breast cancer survival. *J Clin Invest*. 2013 Jun 17. PubMed PMID: 23778140. Pubmed Central PMCID: 3696556.
  48. Loi S, Sirtaine N, Piette F, Salgado R, Viale G, Van Eenoo F, et al. Prognostic and predictive value of tumor-infiltrating lymphocytes in a phase III randomized adjuvant breast cancer trial in node-positive breast cancer comparing the addition of docetaxel to doxorubicin with doxorubicin-based chemotherapy: BIG 02-98. *Journal of clinical oncology : official journal of the American Society of Clinical Oncology*. 2013 Mar 1;31(7):860-7. PubMed PMID: 23341518.
  49. Denkert C, Loibl S, Noske A, Roller M, Muller BM, Komor M, et al. Tumor-associated lymphocytes as an independent predictor of response to neoadjuvant chemotherapy in breast cancer. *J Clin Oncol*. 2010 Jan 1;28(1):105-13. PubMed PMID: 19917869.
  50. Ono M, Tsuda H, Shimizu C, Yamamoto S, Shibata T, Yamamoto H, et al. Tumor-infiltrating lymphocytes are correlated with response to neoadjuvant chemotherapy in triple-negative breast cancer. *Breast cancer research and treatment*. 2012 Apr;132(3):793-805. PubMed PMID: 21562709.
  51. Cyster JG. Chemokines and cell migration in secondary lymphoid organs. *Science (New York, NY)*. 1999 Dec 10;286(5447):2098-102. PubMed PMID: 10617422. Epub 2000/01/05. eng.

## Figure Legends

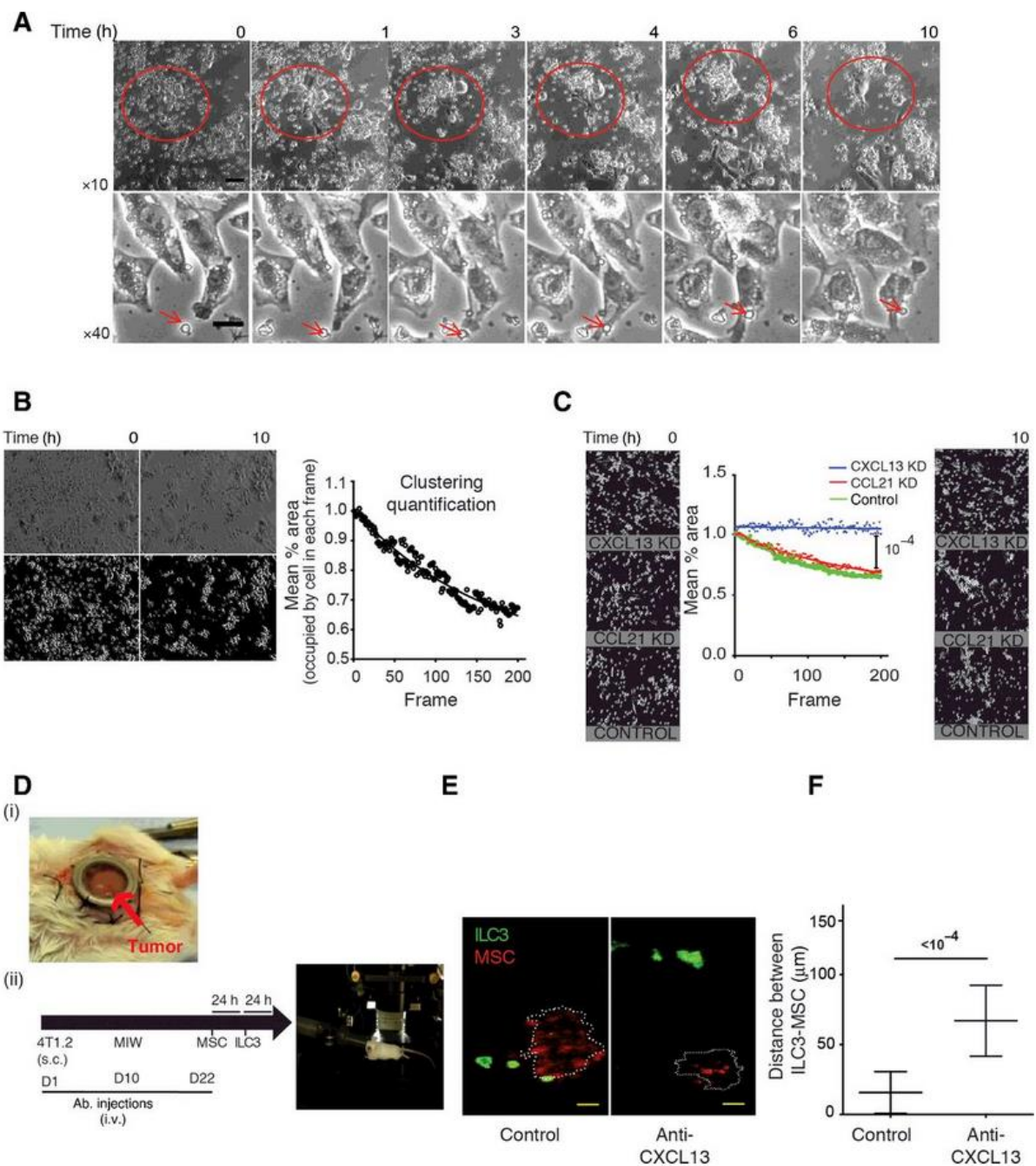
**Figure 1: CCL21 recruits NKp46<sup>+</sup>ILC3 to tumors in a model of TNBC**





**A:** Mice were inoculated subcutaneously with  $10^6$  4T1.2 cells on d0. Control and tumor-bearing mice were culled on d10,12,14,18,20,24. FACS analysis for NKp46<sup>+</sup>ILC3, CD3<sup>+</sup>T and CD19<sup>+</sup>B cells in tumors, DLN and NDLN (n=3/day). **B:** Absolute number of NKp46<sup>+</sup>ILC3 in DLN and NDLN and cell counts/mg of tumor. Confocal micrographs of (C) primary tumor and (D) DLN in BALB/c mice. Yellow arrows point to ILC3. Scale bars=15 $\mu$ m. Absolute number of CD3<sup>+</sup>T cells (E) and CD19<sup>+</sup>B cells (F) in DLN and NDLN and cell counts/milligram of tumor. **G:** CCR7 and CXCR5 expression by intratumoural ILC3, CD3<sup>+</sup> and CD19<sup>+</sup> cells. Levels of CCL21 (H) and CXCL13 (I) in tumors and serum at indicated time points. (n $\geq$ 3/time point). **J:** NKp46<sup>+</sup>ILC3/mg of tumor at d14 after tumor cell implantation, treated with anti-CCL21, anti-CXCL13 or isotype control antibody (n $\geq$ 3). Significance determined by one-way ANOVA and data represent means $\pm$ SEM

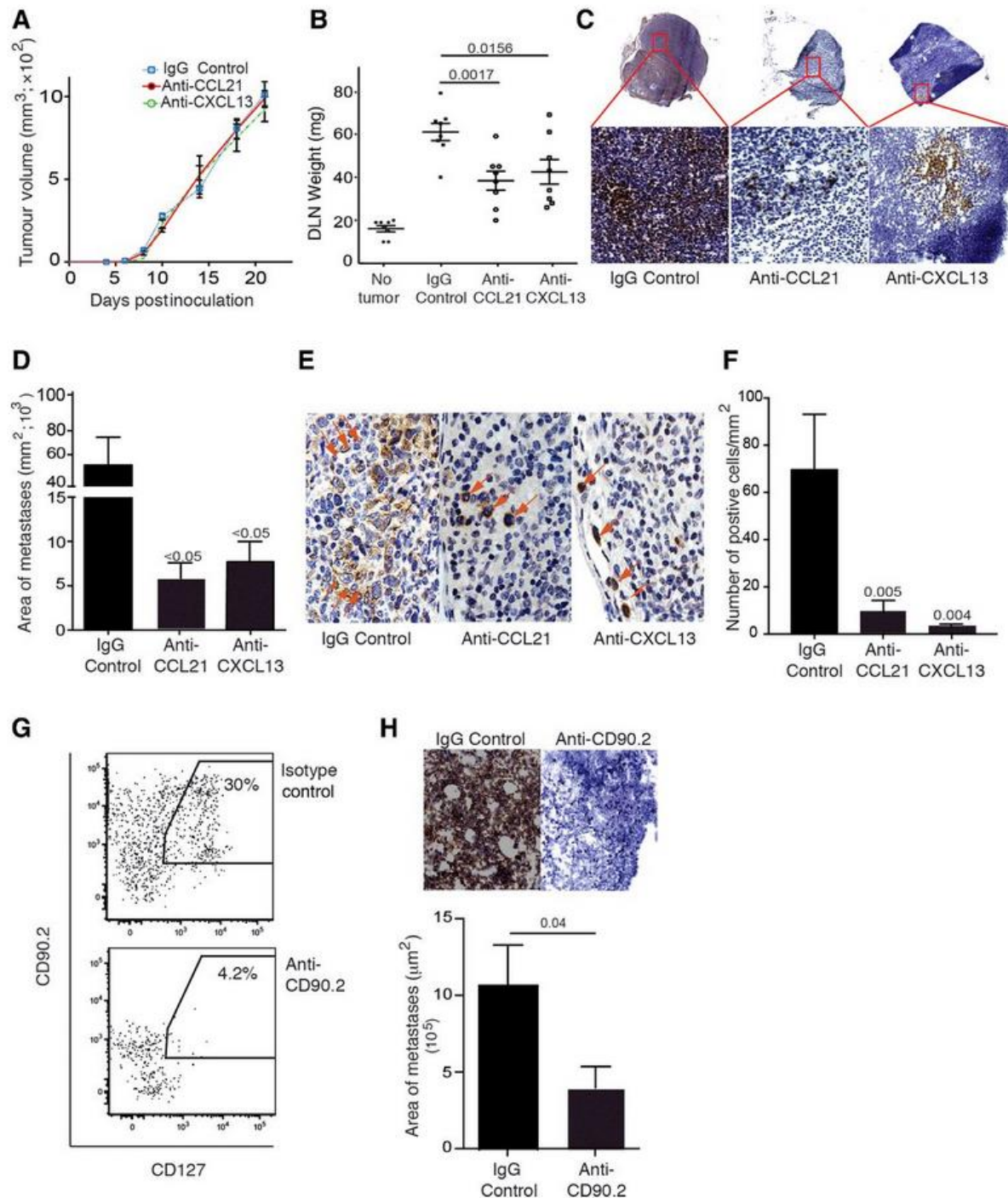
**Figure 2: CXCL13 is required for clustering of NKp46<sup>+</sup>ILC3 and MSC *in vitro* and *in vivo***



**A:** Time-lapse microscopy of sorted splenic ILC3 co-cultured with MSC. Scale bars: upper panel=50 $\mu\text{m}$ ; lower panel=20 $\mu\text{m}$ . **B:** Representative phase contrast (upper panels) and binary images (lower panel) used for the quantification of cell clustering. The graph summarises the change in mean area of the field occupied by cells. **C:** NKp46 ILC3 co-cultured with MSC transfected with siRNA targeting CCL21, CXCL13 or control vector. **D:** i) MIW was surgically implanted on top of the developing tumor. ii) Schematic representation of the experimental plan for multi-photon imaging of MSC-NKp46 ILC3 cell interaction. **E:** Representative images (n=15 fields analyzed). Scale bar=10 $\mu\text{m}$ . **F:**

Mean distances between the centre of imaged MSCs and NKp46<sup>+</sup>ILC3 are shown. Significance was determined using unpaired t-tests.

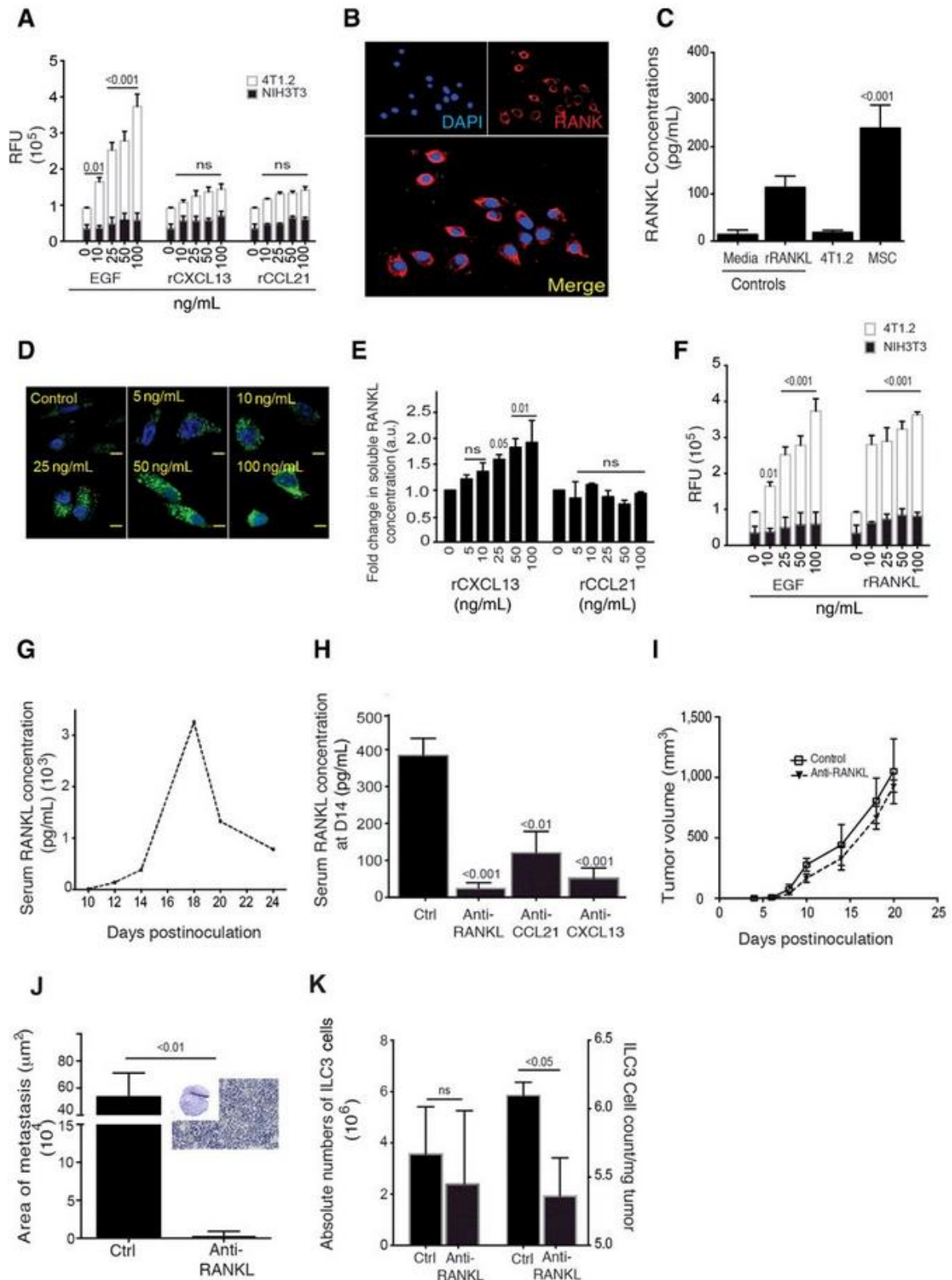
**Figure 3: CCL21, CXCL13 and ILCs promote metastasis of tumor cells to DLN**



Tumour-bearing mice were treated with either anti-CCL21, anti-CXCL13 or isotype control antibodies. n=6 mice per treatment group. **A**: Tumour growth over time. **B**: Weight of inguinal DLN from mice at d21. **C**: Immunohistochemistry (IHC) of DLN from tumour-bearing BALB/c mice at d21 using anti-pancytokeratin (brown). **D**: Quantification of the total area of metastasis per mm<sup>2</sup> of

sectional area within LN at d21. **E:** IHC of DLN from tumour-bearing Rag1<sup>-/-</sup> mice at d21 using anti-pan-cytokeratin (brown). Orange arrows highlight the pan-cytokeratin<sup>+</sup> tumour cells. **F:** Quantification of the total number of pan-cytokeratin<sup>+</sup> tumour cells/mm<sup>2</sup> of sectional area within LN at d21 (n≥3 per group). **G:** FACS analysis for ILC in the DLN of isotype control and anti-CD90.2-treated Rag1<sup>-/-</sup> mice at d14. Gating as in Figure 1A. **H:** Pan-cytokeratin IHC (brown) of DLN of tumour-bearing Rag1<sup>-/-</sup> mice to assess tumour load in ILC-depleted (anti-CD90.2-treated) and non-depleted (isotype control-treated) mice at d21 (bilateral tumors in 3 mice per treatment group (n=6 per treatment group)). The bar graphs show the total area of metastasis per mm<sup>2</sup> of sectional area within LN. Scale Bar=100µm. Data represent means±SEM.

**Figure 4: CXCL13 induces RANK-RANK-L signaling**

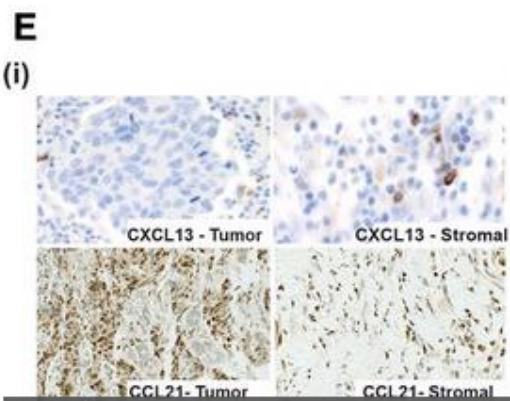
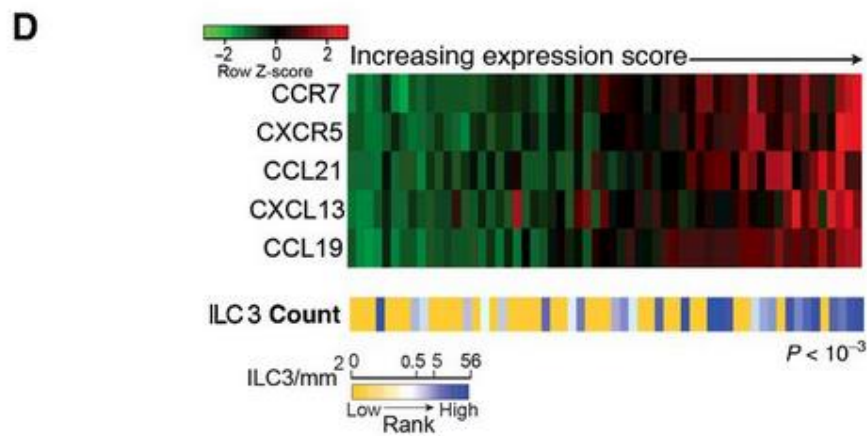
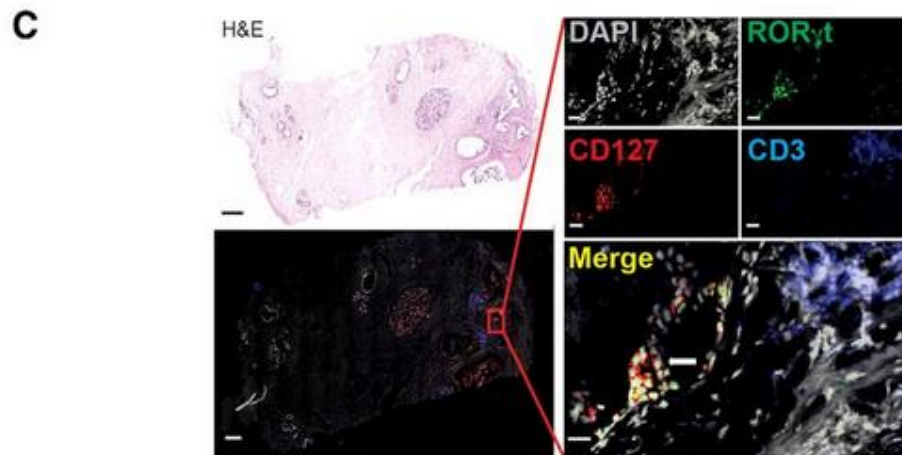
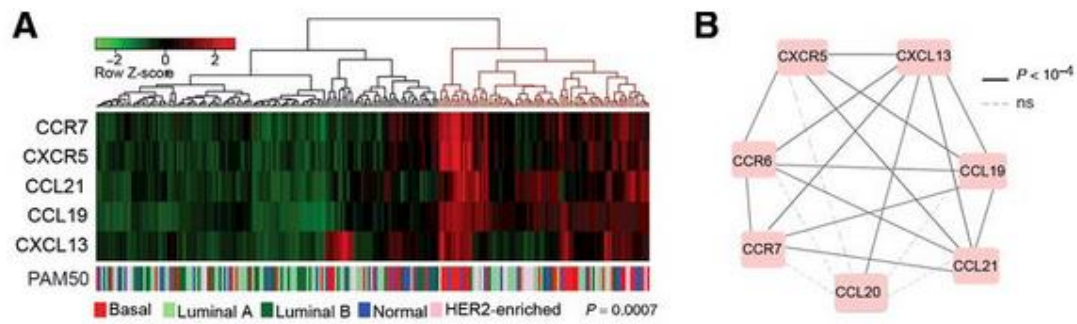


**A:** Cell invasion assay with 4T1.2 cells (white bars) and NIH3T3 cells (black bars, non-invasive control). **B:** Confocal micrograph showing cytoplasmic and membranous staining of RANK (red) in 4T1.2 cells. DAPI-stained nuclei are shown in blue. **C:** Supernatants from co-culture experiments of

4T1.2 cells and MSCs were analysed after 48h to determine RANKL level by ELISA. **D:** RANKL expression in MSCs following stimulation by rCXCL13. Scale bar=50µm. **E:** RANKL concentration in MSC culture supernatants after stimulation with the indicated concentrations of rCXCL13 or rCCL21. Data represent means±SEM, paired t-test. **F:** Cell invasion assay, as described in **A**, with 4T1.2 stimulated with EGF and RANKL. *Note: data on Fig 4A and 4F is the data from the same experiment.* **G:** RANKL serum concentrations were determined at the indicated time points after tumour inoculation. (n=3 mice/timepoint). **H:** RANKL serum concentration at d14 in mice treated with neutralizing antibodies as indicated. Data represent means±SEM, unpaired t-test. **I:** Tumour-bearing mice treated with either anti-RANKL or isotype control antibodies. The change in tumor volume with time after inoculation of 4T1.2 cells into the mammary fat pad is shown. **J:** Quantification of the total area of metastasis/mm<sup>2</sup> of sectional area in DLN of tumour-bearing mice treated with anti-RANKL or isotype control. Inset: representative IHC using anti-pancytokeratin (brown) to assess tumor burden in the anti-RANKL-treated cohort. **K:** Absolute cell counts of NKp46<sup>+</sup>ILC3/milligram of tumour and within DLN from tumour-bearing mice treated with anti-RANKL or isotype control antibody until d21. n≥3 mice/treatment group. (One-way ANOVA. Data represent means±SEM, unpaired t-test).

**Figure 5. RORγt<sup>+</sup>ILC3 and their associated chemokines in the human breast cancer TME.**





(ii)

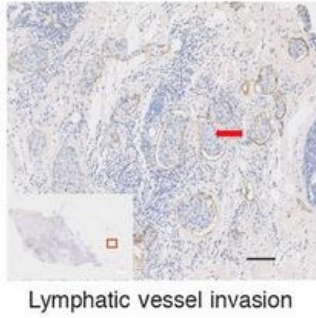
	Number of assessable patients <i>N</i> = 60	(100%)	Number of patients		Fisher exact test ( <i>P</i> value)
			ILC3 Present	ILC3 Absent	
CXCL13					
Positive staining	58	97%	14	6	<i>P</i> = 0.0052
Negative staining			12	26	
CCL21					
Positive staining	50	83%	12	17	<i>P</i> = 0.6609
Negative staining			10	11	



**A:** Hierarchical clustering of the expression of genes encoding lymphoid-associated chemokines and receptors in the Guy's METABRIC data set (n=234). Columns represent patient samples, with dendrogram coloured according to the top-level cut-off point (black/red). PAM50 intrinsic subtype assignments are displayed below and association was determined using a two-tailed Fisher's exact test. **B:** Significance of pair-wise gene expression correlations for genes encoding lymphoid-associated chemokines and receptors. **C:** H&E staining and confocal micrographs of fresh frozen section of a primary human breast cancer. ROR $\gamma$ <sup>+</sup>ILC3 are defined as CD3<sup>-</sup>CD127<sup>+</sup>ROR $\gamma$ <sup>+</sup>. Scale bar=15 $\mu$ m. **D:** Comparison of gene expression profiles and presence of ROR $\gamma$ <sup>+</sup>ILC3. The heatmap illustrates relative expression of genes encoding ROR $\gamma$ <sup>+</sup>ILC3-associated chemokines and receptors. Columns (samples, n=59) are ordered by increasing expression score and rows by hierarchical clustering. The ranks of ILC3 counts (cells/mm<sup>2</sup>) are depicted below, ordered from lowest to highest. **E: i)** IHC analysis for CXCL13 and CCL21 in human breast tumour samples. **ii)** Associations between stromal staining for CXCL13 or CCL21 and the presence/absence of ROR $\gamma$ <sup>+</sup>ILC3. The association of these two cytokines and ILC3 was determined using Fisher's exact test.

**Figure 6: Association of ROR $\gamma$ <sup>+</sup>ILC3 and lymphatic invasion within the TME**

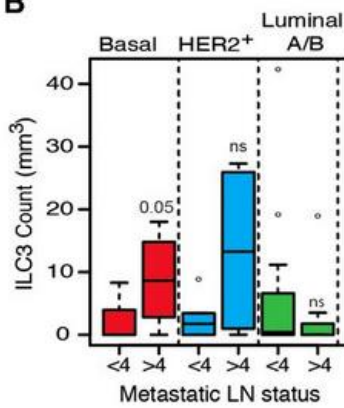
**A**  
(i)



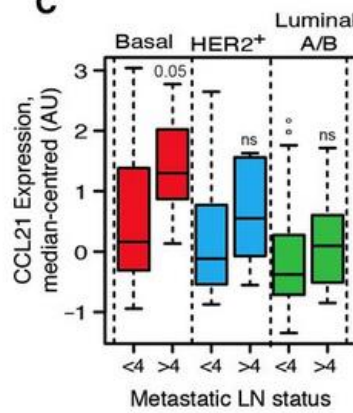
(ii)

	Number of assessable patients <i>N</i> = 60	(100%)	Number of patients Lymphatic invasion		Fisher exact test ( <i>P</i> value)
			Absent	Present	
CD3 <sup>+</sup> Cells					
Low (<100/mm <sup>2</sup> )	49	82%	18	8	<i>P</i> = 0.1548
High (>100/mm <sup>2</sup> )			11	12	
CD3 <sup>+</sup> CD127 <sup>+</sup> RORγT <sup>+</sup> cells					
Absent	48	80%	26	12	<i>P</i> = 0.1446
Present			4	6	
ILC3 Cells					
Absent	47	78%	22	3	<i>P</i> = 0.0003
Present			8	14	

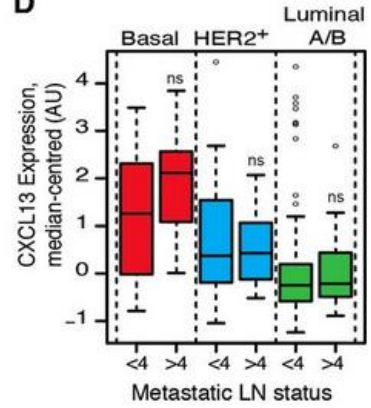
**B**



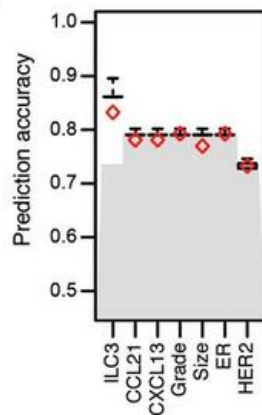
**C**



**D**



**E**



**A: i)** IHC staining with lymphatic marker, podoplanin (brown) in primary human breast cancer tissue, cell nuclei are stained blue. Sections were examined for presence or absence of tumor cell invasion into lymphatics (red arrow) Scale bar=100μm. **ii)** Lymphatic invasion is associated with the presence of RORγt<sup>+</sup>ILC3. The association between numbers of RORγt<sup>+</sup>ILC3, CD3<sup>+</sup>T cells or CD3<sup>+</sup>CD127<sup>+</sup>RORγt<sup>+</sup> cells with lymphatic invasion was determined using Fisher's exact test. CD3 low was defined as <100cells/mm<sup>2</sup>, CD3 high as >100cells/mm<sup>2</sup>. **B:** Correlation between ILC3 count

and the presence of lymphatic metastasis. (Mann Whitney-U-Test, is shown above the boxplots). Correlation between CCL21 (C) and CXCL13 (D) gene expression and lymphatic metastasis in the METABRIC dataset. Median-centred gene expression values are shown (arbitrary units). E: Prediction accuracy for LN burden amongst Basal/HER2-enriched tumours. Average validation accuracy is shown (red diamonds). Baseline accuracy using assignment of all values to the largest class is shown for comparison (grey). ROR $\gamma$ <sup>+</sup>ILC3/mm<sup>2</sup> achieves prediction accuracy of 84% using median threshold of 11.6/mm<sup>2</sup>.

**Figure 7:** In a model of triple negative breast cancer, we report on the CCL21-mediated recruitment of ILC3 to tumors where they stimulate stromal cells to produce CXCL13. CXCL13 feeds back to promote further interactions between ILC3 and stromal cells leading to production of RANKL, which enhances tumor cell motility resulting in lymph node metastases.

